Spectrochimica Acta Part A: Molecular and Biomolecular Spectroscopy 125 (2014) 414–421

Contents lists available at ScienceDirect

Spectrochimica Acta Part A: Molecular and Biomolecular Spectroscopy

journal homepage: www.elsevier.com/locate/saa

Micro-Raman, Mid-IR, Far-IR and DFT studies on 2-[4-(4-Fluorobenzamido)phenyl]benzothiazole

O. Unsalan [a,*], Y. Sert [b,c], H. Ari [d], A. Simão [e], A. Yilmaz [a], M. Boyukata [b], O. Bolukbasi [a], K. Bolelli [f], I. Yalcin [f]

[a] University of Istanbul, Faculty of Science, Physics Department, Vezneciler-Fatih, TR-34134 Istanbul, Turkey
[b] Bozok University, Faculty of Art & Sciences, Physics Department, TR-66100 Yozgat, Turkey
[c] Sorgun Vocational School, Bozok University, Yozgat 66100, Turkey
[d] Bozok University, Faculty of Art & Sciences, Chemistry Department, TR-66200 Yozgat, Turkey
[e] University of Coimbra, Chemistry Department, P-3004-535 Coimbra, Portugal
[f] Ankara University, Department of Pharmaceutical Chemistry, Faculty of Pharmacy, Tandoğan, TR-06100 Ankara, Turkey

HIGHLIGHTS

- BSN-006 is an important compound in drug industry.
- Structure was analyzed by means of DFT/(B3LYP) functional with 6-311++G(d,p) set.
- Far, Mid-infrared and micro-Raman spectroscopic investigations were performed.
- Experimental results are in consistent with the theoretical calculations.
- Hydrogen bonds were also discussed after potential energy scan calculations.

GRAPHICAL ABSTRACT

Optimized geometric structure of BSN-006.

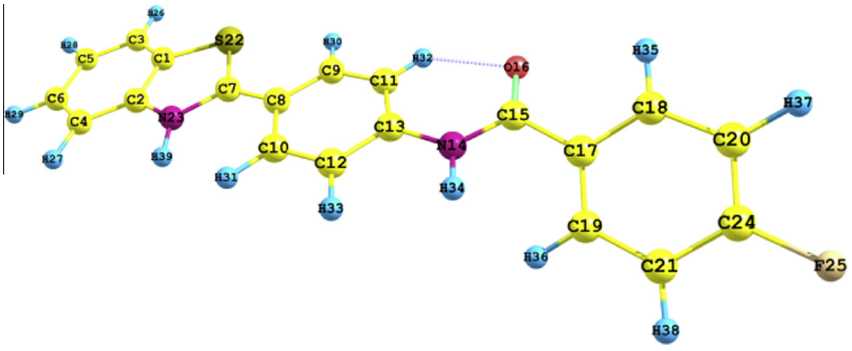

ARTICLE INFO

Article history:
Received 31 July 2013
Received in revised form 23 January 2014
Accepted 27 January 2014
Available online 10 February 2014

Keywords:
2-[4-(4-Fluorobenzamido)phenyl]
benzothiazole
Micro-Raman
Far-infrared
Mid-infrared
DFT
PED

ABSTRACT

Molecular structure of 2-[4-(4-Fluorobenzamido)phenyl]benzothiazole was determined by quantum chemical calculations. MidIR and FarIR spectra were recorded at room temperature, with 4 cm^{-1} resolution in the 4000–400 cm^{-1} and 700–30 cm^{-1} regions, respectively for the first time. Raman spectrum was recorded in the 4000–100 cm^{-1} range. Optimized molecular structure and vibrational wavenumbers of the compound in its ground state have been calculated by using Density Functional Theory using B3LYP functional with 6-311++G(d,p) basis set. Vibrational wavenumbers were seen to be in good agreement with the experimental IR data. Furthermore, assignments of each vibrational mode were interpreted in terms of potential energy distributions in detail.

Introduction

Increasing interest on nano-scale systems in medicinal sciences get the scientists' attentions together from various areas.

* Corresponding author. Address: Department of Physics, Faculty of Science, Istanbul University, Vezneciler, Fatih, 34134, Istanbul, Turkey. Tel.: +90 2124555700; fax: +90 2125190834.
E-mail address: unsalan@istanbul.edu.tr (O. Unsalan).

http://dx.doi.org/10.1016/j.saa.2014.01.118
1386-1425/

Disease-causing microbes that have become resistant to drug therapy are an increasing public health problem. Tuberculosis, gonorrhea, malaria, and childhood ear infections are just a few of the diseases that have become hard to treat with antibiotic drugs. The hospital-acquired infections are resistant to the most powerful antibiotics available, methicillin and vancomycin. These drugs are reserved to treat only the most intractable infections to slow development of resistance to them [1]. So, there is still need for the new classes of antimicrobial agents. The compounds which have benzothiazole nucleus in their structure are involved in research aimed at evaluating new chemotherapeutically active agents, such as antimicrobial [2–5], a topical carbonic anhydrase inhibitor [6], a cyclooxygenase inhibitor [7], antitubercular [8,9] anti-nematode [10], a dual inhibitor of thromboxane A2 synthetase and 5-lipoxygenase [11], a selective and reversible inhibitor of monoamine oxidase type A (MAO-A) [12], antiallergic [13], multi-drug resistance cancer cell activities with inhibiting activity on eukaryotic topoisomerase II enzyme in cell-free system, eukaryotic topoisomerase II inhibitor exhibiting a better inhibitor activity than reference drug etoposide [14–16] and antitumor agents [17–19]. Currently, a new series of benzothiazoles have been synthesized as antitumor agents and showed potential inhibitory activity against human breast cancer cell lines *in vitro* and *in vivo* [17]. Among them, lysylamide of 2-(4-amino-3-methylphenyl)-5-fluorobenzothiazole had been selected for phase 1 clinical evaluation [18]. Recently, it has been reported the synthesis of several 2-substitutedbenzothiazole derivatives as the antimicrobial agents [20,21]. According to these studies, the compounds were found to have inhibitory effect with minimum inhibitory concentration (MIC) value of 3.12–50 μg/ml against some of Gram-positive, Gram-negative bacteria and Candida albicans as yeast. Among the tested compounds, 2-(phenoxymethyl)benzothiazole was found as the most active derivative at a MIC value of 3.12 μg/ml against the tested S. aureus [21]. In spite of the existing studies, there are still lack of information about structural and energetic properties of *2-[4-(4-Fluorobenzamido)phenyl]benzothiazole*. Therefore, in this work, the title molecule ($C_{20}H_{14}N_2SOF$) has been computationally investigated by using Density Functional Theory (DFT). Moreover, the results have been confirmed via experimental analysis.

Computational details

Calculation for optimizing the stable structure of the molecule was performed in Gaussian09 [22], using DFT/B3LYP functional with 6-311++G(d,p) basis set. Calculated harmonic vibrational wavenumbers were scaled down by a single factor of 0.978, to correct them for the systematic shortcomings of the applied methodology (mainly for anharmonicity). The vibrational modes were assigned in detail on the basis of Potential Energy Distribution (PED) analysis using VEDA [23] software. Optimized geometry from the output file of the calculation was visualized with ChemCraft software [24].

Experimental details

IR Spectra

All MidInfrared (MIR) and FarInfrared (FIR) spectra of the compound were recorded at room temperature, with 4 cm^{-1} resolution, between 4000–400 cm^{-1} and with a humidity/temperature controlled system. MIR spectra of the compound were recorded by KBr method (grounded in a mortar) and Attenuated Total Reflectance (ATR, with diamond crystal) technique on FT/IR-420 spectrometer and Perkin Elmer Spectrum Two spectrometer, respectively. Besides, FIR spectrum was recorded between 700 and 30 cm^{-1}, on a Perkin Elmer Spectrum-400 spectrometer, by ATR technique, for the first time. To collect all spectra, solid sample of *2-[4-(4-Fluorobenzamido)phenyl]benzothiazole* (BSN-006) [25] was simply placed on ATR unit's diamond surface. Up to our knowledge, there has not been any study of MIR, FIR, Raman, DFT and crystallographic studies on BSN-006 yet.

Raman spectrum

The Raman spectrum was recorded on Renishaw Invia Raman spectrometer in the 4000–100 cm^{-1} region. The excitation source was 785 nm line of a diode laser with 3.1 μm estimated laser spot size, magnification of 50× of the microscope 20 μm slit aperture and 32 accumulations for each measurement. Raman spectrum was also recorded due to its complementarity to both MIR and FIR in order to identify some bands which do not appear neither in MIR nor FIR spectra.

Results and discussion

Molecular geometry

Because of having neither reflection plane nor inversion center, calculations utilized the C_1 symmetry of BSN-006. It contains benzothiazole part with one S atom and one N atom in the thiazole ring. Henceforth, for the clarity, the rings will be named as A for the ring connected to thiazole ring, B for thiazole ring, C for central phenyl ring and D for the benzene ring containing F atom. The atom numbering scheme and optimized geometry of BSN-006 is shown in Fig. 1. The structural parameters; bond lengths, bond angles and selected dihedral angles (N_{14}—C_{15}—C_{17}—C_{19}, the angle between ring C and D, and the dihedral (C_{15}—$O_{16}\cdots H_{32}$—C_{11}) between C═O bond and C—H bond of Ring C (involving in formation of Hydrogen bond (HB) together) of BSN-006 were tabulated in Table 1. The bond lengths, bond angles and dihedral angle for BSN-006 were computed at DFT level of theory and with B3LYP functional with 6-311++G(d,p) basis set. Identification of molecular structure of BSN-006 and recording different spectra of BSN-006 are important because it can be the basis for distinguishing the derived analogs, as a further study, of BSN-006 from each other. For this reason, quantum chemical calculation on BSN-006 was also performed. By taking into account the fact that the molecular geometry in the gas phase may be different from that in its solid phase, owing to extended Hydrogen bonding and stacking interactions it can be seen that there is a reasonable agreement between calculated and experimental vibrational wavenumbers. On the other hand, due to there is no experimental structural data on this compound, only computational results were presented in this study. Calculations show that the optimized structure of BSN-006 has one HB formed at the distance of 2.236 Å between $O_{16}\cdots H_{32}$ as expected. In Table 1, other possible HB's according to the most stable four conformers (conf1–4) of BSN-006 were also given. D ring is bended from the plane with a dihedral angle of 26.3° and angle between the planes which are constructed by C═O bond and $C_{11}H_{32}$ bond of the ring C, is 12.9°.

The bond between C_{13} and N_{14} is not as flexible as the bond between C_{15} and C_{17} due to the HB between O_{16} and H_{32}. Therefore, the dihedral angle N_{14}—C_{15}—C_{17}—C_{19}, 26.3°, is larger than that one of C_{15}—$O_{16}\cdots H_{32}$—C_{11}, 12.9°. Additionally, the Hydrogen atoms H_{33} and H_{34} repel each other due to their positively-charged states. This repelling force is more than the repulsive force between H_{34} and H_{36} since the oriantation of the D ring is not in the same plane with respect to the main plane of BSN-006. This explanation based on structural and repulsive effects can also be confirmed through analysing the atomic charge distributions on the atoms in the considered sites of BSN-006.

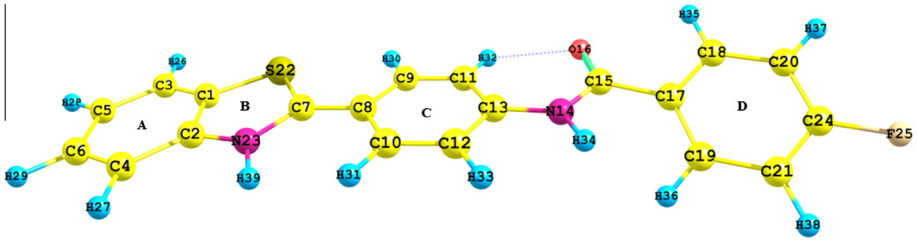

Fig. 1. Optimized geometric structure of BSN.

Table 1
Optimized geometric parameters of BSN-006 and Hydrogen bonding parameters according to the conformers.

							Conf1	Conf2	Conf3	Conf4
Bond Lengths in Ångström (Å)										
R(1–2)	1.405	R(6–29)	1.084	R(11–32)	1.079	R(18–35)	1.083	–	–	–	–
R(1–3)	1.388	R(7–8)	1.409	R(12–13)	1.406	R(19–21)	1.393	–	–	–	–
R(1–22)	1.774	R(7–22)	1.773	R(12–33)	1.087	R(19–36)	1.084	–	–	–	–
R(2–4)	1.396	R(7–23)	1.390	R(13–14)	1.409	R(20–24)	1.387	–	–	–	–
R(2–23)	1.382	R(8–9)	1.424	R(14–15)	1.375	R(20–37)	1.083	–	–	–	–
R(3–5)	1.398	R(8–10)	1.425	R(14–34)	1.008	R(21–24)	1.386	–	–	–	–
R(3–26)	1.083	R(9–11)	1.381	R(15–16)	1.223	R(21–38)	1.083	–	–	–	–
R(4–6)	1.395	R(9–30)	1.084	R(15–17)	1.503	R(23–39)	1.007	–	–	–	–
R(4–27)	1.084	R(10–12)	1.380	R(17–18)	1.401	R(24–25)	1.353	–	–	–	–
R(5–6)	1.396	R(10–31)	1.084	R(17–19)	1.401	R(16–32)[a]	2.236	2.232	2.238	4.738[b]	3.901[b]
R(5–28)	1.083	R(11–13)	1.408	R(18–20)	1.390	R(16–35)[a]	2.504[b]	2.502	2.501	2.571	2.563
Bond angles in (°)										
A(2–1–3)	121.0	A(4–6–29)	119.2	A(10–12–13)	121.5	A(17–18–20)	120.9				
A(2–1–22)	110.9	A(6–5–28)	120.0	A(10–12–33)	119.0	A(17–18–35)	118.4				
A(1–2–4)	120.2	A(5–6–29)	119.7	A(13–11–32)	119.4	A(17–19–21)	120.9				
A(1–2–23)	112.3	A(8–7–22)	125.1	A(11–13–12)	118.5	A(17–19–36)	120.8				
A(3–1–22)	128.1	A(8–7–23)	125.5	A(11–13–14)	124.0	A(20–18–35)	120.6				
A(1–3–5)	118.7	A(7–8–9)	121.6	A(11–32–16)	118.7	A(18–20–24)	118.5				
A(1–3–26)	120.7	A(7–8–10)	122.1	A(13–12–33)	119.5	A(18–20–37)	121.7				
A(1–22–7)	91.1	A(22–7–23)	109.4	A(12–13–14)	117.6	A(21–19–36)	118.2				
A(4–2–23)	127.4	A(7–23–39)	121.1	A(13–14–15)	129.1	A(19–21–24)	118.4				
A(2–4–6)	118.6	A(9–8–10)	116.3	A(13–14–34)	114.7	A(19–21–38)	121.7				
A(2–4–27)	120.6	A(8–9–11)	122.4	A(15–14–34)	116.0	A(24–20–37)	119.8				
A(2–23–7)	116.2	A(8–9–30)	119.4	A(14–15–16)	123.7	A(20–24–21)	122.3				
A(2–23–39)	121.8	A(8–10–12)	121.2	A(14–15–17)	115.1	A(20–24–25)	118.9				
A(5–3–26)	120.6	A(8–10–31)	120.8	A(16–15–17)	121.3	A(24–21–38)	119.9				
A(3–5–6)	120.4	A(11–9–30)	118.2	A(15–16–32)	103.9	A(21–24–25)	118.8				
A(3–5–28)	119.6	A(9–11–13)	120.2	A(15–17–18)	117.2						
A(6–4–27)	120.8	A(9–11–32)	120.4	A(15–17–19)	124.0						
A(4–6–5)	121.1	A(12–10–31)	118.0	A(18–17–19)	118.9						
Dihedral angles in (°)										
D (14–15–17–19)	26.3	D (15–16–32–11)	12.9	D (12–13–14–34)	0.1	D (15–17–18–35)	0.3				

[a] Hydrogen bond lengths according to the conformer numbers (**A**···**H**), A: H bonded electronegative atom,
[b] No Hydrogen bond.

In general, two C—S bond lengths were calculated 1.774 Å and 1.773 Å in the ring B. Two C—N bond lengths in the ring B were calculated 1.382 Å and 1.390 Å. C—C bond length in ring B is 1.405 Å. N—H bond length in ring B was calculated 1.007 Å and other N—H bond length was calculated (C=O—NH) as 1.008 Å. Carbonyl (C=O) bond length, which also involves in HB, was calculated 1.223 Å. C—F bond length in D was calculated as 1.353 Å. Both C—C bond between B and C rings and C—N bond connects to ring D via C=O—NH linkage were calculated as 1.409 Å. Bond length of C—N bond, which is in connection to carbonyl group, is 1.375 Å. C—C bond lengths in ring A were calculated between 1.386 Å and 1.405 Å. C—C bonds' lengths were calculated between 1.380 Å and 1.424 Å. C—H bond lengths in ring A; were calculated between 1.083 Å and 1.084 Å, in ring C; between 1.079 Å and 1.084 Å, in ring D; 1.083 Å and 1.084 Å, respectively.

Regarding the bond angles, C—N—C bond angle in ring B, C—S—C in ring B, C—C—S between rings B and C, N—C=O bond angle, C—C=O bond angle, C—C—F in D were calculated as 116.2°, 91.1°, 125.1°, 117.6°, 123.7°, 121.3° and 118.9°, respectively. All C—C—H angles of BSN-006 were calculated between 118.4° and 121.7°.

Vibrational assignments for MIR, Raman and FIR spectra

Experimental and computational vibrational wavenumbers were given in Table 2, together with the Potential Energy Distribution (PED) values.

FIR spectroscopy is also a complementary technique to the MIR and also allow to assign the calculated wavenumbers especially below 450 cm^{-1} [26]. FIR spectrum also was seen in good agreement with the wavenumbers observed in Raman spectra. FIR spectrum of BSN-006 was recorded between 700–30 cm^{-1} and given in Fig. 2. MIR and calculated MIR spectra were given in Fig. 3 and Raman spectrum in Fig. 4, respectively.

Table 2
FIR, Raman, MIR (both with KBr and ATR techniques) and computational wavenumbers (cm^{-1}) and PED values of BSN-006.

No.	FIR[a]	Raman	Exp. KBr	Exp. ATR	Calc.	Scaled.	PED (%)[b]
1	–	3562vw	3351w	3351w	3648	3568	υNH(100) N_{23}—H_{39} (B)[c]
2	–	–	–	–	3623	3543	υNH(100) N_{14}—H_{34}
3	–	–	–	3179w	3242	3171	υCH(100) C_{11}—H_{32} (C)
4	–	–	–	3138w	3208	3137	υCH(100) C_{18}—H_{35}, C_{20}—H_{37} (D)
5	–	–	–	–	3202	3132	υCH(99) C_{21}—H_{38}, C_{19}—H_{36}, C_{20}—H_{37} (D)
6	–	–	–	–	3198	3128	υCH(86) C_6—H_{29}, C_5—H_{28}, C_4—H_{27}, C_3—H_{26} (A)
7	–	–	–	–	3195	3125	υCH(97) C_{18}—H_{35}, C_{20}—H_{37} (D)
8	–	–	–	–	3187	3117	υCH(94) C_3—H_{26}, C_4—H_{27}, C_6—H_{29} (A)
9	–	–	–	3110w	3178	3108	υCH(87) C_3—H_{26}, C_4—H_{27}, C_5—H_{28} (A)
10	–	–	–	–	3171	3101	υCH(91) C_{10}—H_{31}, C_{12}—H_{33} (C)
11	–	–	–	–	3170	3100	υCH(98) C_{19}—H_{36}, C_{21}—H_{38} (D)
12	–	–	–	–	3169	3099	υCH(100) C_3—H_{26}, C_4—H_{27}, C_6—H_{29}, C_5—H_{28} (A)
13	–	–	–	–	3168	3098	υCH(100) C_9—H_{30} (C)
14	–	3067vw	3041vw	3060w	3143	3074	υCH(100) C_{12}—H_{33}, C_{10}—H_{31} (C)
15	–	1655vw	1653vs	1652vs	1715	1677	υOC(77) O_{16}—C_{15}
16	–	1606m	1602s	1601m	1641	1605	υCC(35) C_{18}—C_{20}, C_{19}—C_{21} (D) + δHCC(18) H_{38}—C_{21}—C_{19} (D)
17	–	–	–	–	1628	1592	υCC(44) C_2—C_4 (A)
18	–	1590w	1589s	1590m	1626	1590	υCC(44) C_{17}—C_{19} (D)
19	–	–	–	–	1618	1582	υCC(30) C_{12}—C_{10}, C_5—C_6 (C, A) + δHCC(13) H_{27}—C_4—C_6, H_{38}—C_{21}—C_{19} (A, D)
20	–	–	–	–	1615	1579	υCC(37) C_1—C_3, C_{10}—C_{12} (A, C)
21	–	1557vw	–	1556vw	1589	1554	δHNC(35) H_{34}—N_{14}—C_{13} + υCC(17) C_{12}—C_{13} (C)
22	–	1519vw	1516m	1517vw	1557	1523	δHCC(17) H_{30}—C_9—C_8 (C) + υCC(15) C_7—C_8 + υNC(11) N_{23}—C_2 (B) + δHNC(10) H_{39}—N_{23}—C_7 (C)
23	–	1500vw	1502m	1503m	1535	1501	δHCC(45) H_{35}—C_{18}—C_{17} (D) + υCC(16) C_{17}—C_{18} (D)
24	–	1481vs	1483m	1483m	1518	1485	υCC(24) C_8—C_{10} (C) + δHNC(18) H_{34}—N_{14}—C_{13} + δHCC(16) H_{32}—C_{11}—C_9 (C)
25	–	–	–	–	1507	1474	δHCC(23) H_{28}—C_5—C_6, H_{32}—C_{11}—C_{13} (A, C) + δHNC(11) H_{39}—N_{23}—C_2 (B)
26	–	1456s	1456w	1455w	1495	1462	δHCC(32) H_{27}—C_4—C_6 (A) + δCCC(26) C_1—C_2—C_4 (A)
27	–	1436s	1435m	1434m	1466	1434	δHCC(41) H_{29}—C_6—C_4 (A)
28	–	1411vw	–	–	1448	1416	υCC(45) C_9—C_{11}, C_{10}—C_{12} (C) + δHCC(29) H_{30}—C_9—C_8 (C)
29	–	1388vw	1408w	1404w	1433	1401	δHCC(31) H_{35}—C_{18}—C_{17} (D) + υCC(14) C_{18}—C_{20} (D)
30	–	1382vw	–	1358vw	1394	1363	υCC(23) C_3—C_5 (A), C_7—C_8 + δHNC(17) H_{39}—N_{23}—C_2 + υNC(12) N_{23}—C_2 (B)
31	–	1324w	1327w	1324m	1340	1311	δHCC(58) H_{32}—C_{11}—C_{13} (C) + υNC(11) N_{14}—C_{13}
32	–	1307w	–	–	1336	1307	υCC(67) C_{20}—C_{24} (D)
33	–	–	–	–	1333	1304	υCC(37) C_1—C_2, C_{11}—C_{13} (A, C)
34	–	–	–	–	1327	1298	υCC(35) C_8—C_9, C_5—C_6 (A, C) + δHCC(14) H_{26}—C_3—C_1 (A)
35	–	1285vw	1284w	1287w	1320	1291	δHCC(77) H_{37}—C_{20}—C_{24} (D)
36	–	1262w	1262w	1262w	1284	1256	υNC(24) N_{23}—C_2 (B) + υCC(12) C_1—C_2 (A)
37	–	1248w	1252w	–	1281	1253	δHNC(23) H_{39}—N_{23}—C_2+δHCC(22) H_{24}—C_4—C_2
38	–	–	–	–	1267	1239	υNC(32) N_{14}—C_{13}
39	–	1230w	1232m	1229m	1252	1224	υCC(21) C_{15}—C_{17} + δHNC(17) H_{34}—N_{14}—C_{15} + υNC(12) N_{14}—C_{15}
40	–	–	–	–	1244	1217	υFC(44) F_{25}—C_{24} + δHCC(21) H_{35}—C_{18}—C_{20}, H_{36}—C_{19}—C_{21}
41	–	1182m	1181w	1181m	1217	1190	δHCC(29) H_{32}—C_{11}—C_{13} + υNC(21) N_{23}—C_7
42	–	1161vw	1171w	1170m	1190	1164	δHCC(46) H_{31}—C_{10}—C_{12}, H_{33}—C_{12}—C_{13}
43	–	–	1161w	–	1182	1156	δHCC(71) H_{27}—C_4—C_6, H_{26}—C_3—C_5, H_{29}—C_6—C_5, H_{28}—C_5—C_6+υCC(14) C_5—C_6
44	–	1150vw	–	–	1177	1151	δHCC(63) H_{37}—C_{20}—C_{24}, H_{38}—C_{21}—C_{24}, H_{35}—C_{18}—C_{20}, H_{36}—C_{19}—C_{21}
45	–	1127vw	1126vw	1128vw	1146	1121	δHCC(37) H_{30}—C_9—C_8
46	–	–	1118vw	–	1143	1118	δHCC(40) H_{26}—C_3—C_1+υCC(37) C_3—C_5, C_4—C_6
47	–	–	1107vw	1108w	1125	1100	δHCC(50) H_{35}—C_{18}—C_{17}
48	–	1106vw	1096vw	1096w	1114	1089	υNC(18) N_{14}—C_{15} + υCC(14) C_{17}—C_{18} + δHCC(12) H_{36}—C_{19}—C_{17}
49	–	1055vw	–	1043vw	1075	1051	δCCC(27) C_1—C_2—C_4, C_3—C_5—C_6
50	–	1016vw	1013vw	1014w	1042	1019	υCC(49) C_5—C_6 + δHCC(17) H_{26}—C_3—C_1
51	–	–	–	–	1029	1006	δCCC(52) C_{18}—C_{17}—C_{19}, C_{20}—C_{24}—C_{21}, C_{17}—C_{18}—C_{20} + δHCC(24) H_{38}—C_{21}—C_{19}
52	–	993vw	–	990vw	1008	986	δCCC(62) C_{11}—C_{13}—C_{12}, C_9—C_8—C_{10}, C_9—C_{11}—C_{13} + δHCC(14) H_{32}—C_{11}—C_{13}
53	–	974vw	970m	971m	988	966	τHCCC(87) H_{35}—C_{18}—C_{17}—C_{19}, H_{37}—C_{20}—C_{18}—C_{17} out of H (D)
54	–	–	–	–	978	956	τHCCC(75) H_{30}—C_9—C11—C_{13}, H_{32}—C_{11}—C_{13}—C_{12} out of H (C)
55	–	944vw	–	–	967	946	τHCCC(77) H_{29}—C_6—C5—C_3 out of H (A)
56	–	–	–	943vw	963	942	δCCC(23) C_7—C_8—C_9, C_{11}—C_{13}—C_{12} + υCC(11) C_8—C_9
57	–	–	936vw	937vw	954	933	τHCCC(77) H_{36}—C_{19}—C_{17}—C_{18}, H_{38}—C_{21}—C_{19}—C_{17} out of H (D)
58	–	–	–	913vw	924	904	τHCCC(87) H_{31}—C_{10}—C_{12}—C_{13}, H_{33}—C_{12}—C_{13}—C_{11} out of H (C)
59	–	902vw	899vw	899vw	915	895	τHCCC(87) H_{27}—C_4—C_6—C_5 out of H (A)
60	–	865vw	–	–	904	884	δOCN(26) O_{16}—C_{15}—N_{14} + δCNC(16) C_{13}—N_{14}—C_{15} + υCC(12) C_{15}—C_{17}
61	–	850vw	850m	849s	866	847	δCCC(34) C_3—C_5—C_6 + υCC(13) C_1—C_2
62	–	–	842m	842s	865	846	τHCCC(51) H_{37}—C_{20}—C_{24}—C_{21} out of H (D) + τFCCC(14) F_{25}—C_{24}—C_{21}—C_{19}
63	–	831vw	830m	830s	840	822	υCC(20) C_{11}—C_{13}
64	–	–	–	–	837	819	τHCCC(78) H_{27}—C_4—C_6—C_5 out of H
65	–	806vw	804w	805m	827	809	τHCCC(85) H_{38}—C_{21}—C_{24}—C_{20} out of H
66	–	–	–	–	814	796	υCC(24) C_{11}—C_{13}, C_{12}—C_{13} + υFC(12) F_{25}—C_{24}
67	–	–	–	786vw	811	793	τHCCC(75) H_{30}—C_9—C_8—C_{10} out of H
68	–	761vw	758s	758vs	769	752	τHCCC(89) H_{30}—C_9—C_8—C_{10} out of H
69	–	741vw	–	–	760	743	γONCC(45) O_{16}—N_{14}—C_{15}—C_{17}
70	–	722vw	728s	729m	744	728	τHCCC(90) H_{29}—C_6—C_5—C_3 out of H
71	–	697vw	701w	701w	713	697	τCCCC(57) C_1—C_2—C_3—C_4, C_{10}—C_8—C_9—C_{11} out of C
72	–	–	–	–	710	694	δCCC(51) C_2—C_1—C_3, C_4—C_6—C_5+δSCN(15) S_{22}—C_7—N_{23}
73	692vw	692vw	691w	–	708	692	τCCCC(54) C_1—C_2—C_3—C_4 out of C
74	685vw	–	–	–	693	678	γONCC(20) O_{16}—N_{14}—C_{15}—C_{17} + τCCCC(14) C_{17}—C_{19}—C_{18}—C_{20}

(*continued on next page*)

Table 2 (*continued*)

No.	FIR[a]	Raman	Exp. KBr	Exp. ATR	Calc.	Scaled.	PED (%)[b]
75	663w	–	663w	661w	685	670	υSC(31) S_{22}—C_7 + δCNC(14) C_2—N_{23}—C_7
76	647m	–	–	648m	657	643	δCCC(21) C_9—C_8—C_{10}
77	–	629vw	–	–	646	632	δCCC(47) C_{18}—C_{20}—C_{24}, C_{19}—C_{21}—C_{24}, C_{17}—C_{18}—C_{20} + υCC(15) C_{18}—C_{20} + δFCC(10) F_{25}—C_{24}—C_{21}
78	622s	622vw	620w	622m	642	628	δCCC(51) C_8—C_9—C_{11}, C_8—C_{10}—C_{12}
79	601s	600vw	600w	600m	607	594	δCCC(24) C_{20}—C_{24}—C_{21} + υCC(11) C_{15}—C_{17} + δOCN(10) O_{16}—C_{15}—N_{14}
80	562w	561vw	–	561vw	568	556	τHNCC(19) H_{34}—N_{14}—C_{15}—C_{17} + δCCC(14) C_1—C_2—C_4
81	551s	552vw	540vw	–	556	544	τHNCC(71) H_{34}—N_{14}—C_{13}—C_{12}
82	533vw	542vw	551m	551m	543	531	τCCCC(60) C_3—C_5—C_6—C_4 out of C (A)
83	511vs	507vw	502m	510s	514	503	γFCCC(27) F_{25}—C_{24}—C_{20}—C_{18} + τHCCC(20) H_{38}—C_{21}—C_{19}—C_{24} out of H (D)
84	499w	–	497m	500m	502	491	γCNCC(56) C_{15}—N_{14}—C_{13}—C_{11}
85	472w	–	465vs	465vw	497	486	δSCN(36) S_{22}—C_7—N_{23}
86	456w	457vw	456m	458vw	455	445	δCCC(10) C_{19}—C_{17}—C_{15}
87	440m	431vw	426s	–	431	422	δCNC(12) C_{13}—N_{14}—C_{15} + δCCN(10) C_{12}—C_{13}—N_{14}
88	–	–	–	–	425	416	τCCCC(40) H_{38}—C_{21}—C_{19}—C_{24} out of H (D)
89	420w	420vw	418w	–	424	415	τCCCC(32) H_{26}—C_3—C_1—C_5, H_{38}—C_{21}—C_{19}—C_{24} out of H (A, D)
90	401m	415vw	408w	–	417	408	τCCCC(70) C_9—C_8—C_{10}—C_{12}, C_{12}—C_{13}—C_{11}—C_9 + τHCCC(19) H_{32}—C_{11}—C_{13}—C_9
91	385w	384vw	–	–	401	392	δFCC(41) F_{25}—C_{24}—C_{21}
92	369m	368vw	–	–	382	374	γSNCC(20) S_{22}—N_{23}—C_7—C_8 + τCCNC(11) C_{11}—C_{13}—N_{23}—C_{15}
93	355vw	358vw	–	–	368	360	δCCN(33) C_{11}—C_{13}—N_{14} + δOCN(17) O_{16}—C_{15}—N_{14}
94	312m	317vw	–	–	320	313	γCCCC(13) C_{19}—C_{21}—C_{15}—C_{24} out of C (D)
95	–	–	–	–	309	302	δCCC(12) C_7—C_8—C_9 + δCCN(10) C_1—C_2—N_{23}
996	295m	298vw	–	–	298	291	γSNCC(11) S_{22}—N_{23}—C_7—C_8
97	275vw	–	–	–	281	275	τCCCC(24) C_{17}—C_{19}—C_{21}—C_{24} out of C (D)
98	–	267vw	–	–	266	260	τHNCC(60) H_{39}—N_{23}—C_1—C_2 + τCCCC(10) C_3—C_1—C_2—C_4
99	241w	–	–	–	242	237	τCCCC(22) C_1—C_3—C_5—C_6 + τHNCC(15) H_{39}—N_{23}—C_7—C_8 + τCNCC(13) C_{13}—N_{14}—C_{15}—C_{17}
100	212m	213vw	–	–	215	210	δCCC(23) C_{15}—C_{17}—C_{18} + δCCN(13) C_{12}—C_{13}—N_{14}
101	173m	177vw	–	–	177	173	τCCNC(38) C_4—C_2—N_{23}—C_7 + τCCCC(14) C_1—C_2—C_4—C_6 + τCNCC(10) C_{15}—N_{14}—C_{13}—C_{11} + γSNCC(10) S_{22}—N_{23}—C_7—C_8
102	147m	155vw	–	–	149	146	τCCNC(14) C_{11}—C_{13}—N_{14}—C_{15}
103	136m	135w	–	–	141	138	δCNC(11) C_{13}—N_{14}—C_{15} + τCCNC(10) C_{11}—C_{13}—N_{14}—C_{15}
104	100s	111w-sh	–	–	102	100	τCCNC(20) C_{11}—C_{13}—N_{14}—C_{15} + γCCCC(11) C_{15}—C_{17}—C_{18}—C_{20}
105	81vs	–	–	–	88	86	γCCCC(13) C_{15}—C_{17}—C_{18}—C_{20} + δCNC(13) C_{13}—N_{14}—C_{15}
106	72m	–	–	–	68	67	τCNCC(44) C_{13}—N_{14}—C_{15}—C_{17}, C_{15}—N_{14}—C_{13}—C_{11}, C_{15}—N_{14}—C_{13}—C_{12}
107	52m	–	–	–	53	52	τCNCC(61) C_{15}—N_{14}—C_{13}—C_{12} + τCCNC(11) C_{11}—C_{13}—N_{14}—C_{15}
108	44m	–	–	–	42	41	τCNCC(45) C_2—N_{23}—C_7—C_8, C_{13}—N_{14}—C_{15}—C_{17} + δCNC(17) C_2—N_{23}—C_7
109	37m	–	–	–	35	34	δCNC(19) C_{13}—N_{14}—C_{15} + τCNCC(13) C_2—N_{23}—C_7—C_8 + τCCNC(13) C_{11}—C_{13}—N_{14}—C_{15}
110	–	–	–	–	21	21	τCCNC(52) C_{11}—C_{13}—N_{14}—C_{15} + τCNCC(26) C_2—N_{23}—C_7—C_8
111	–	–	–	–	17	17	τCNCC(58) C_{13}—N_{14}—C_{15}—C_{17} + τCCNC(13) C_2—N_{23}—C_7—C_8 + τCCCC(10) C_{15}—C_{17}—C_{19}—C_{21}

[a] FIR (Far Infrared);
[b] PED (Potential Energy Distribution) values lower than 10% were not included notations for the approximate experimental MIR and FIR intensity values given here are: vw: very weak, w: weak, m: medium, s: strong, vs: very strong, sh: shoulder.
[c] Letters in parentheses stand for the rings, i.e. (A) for ring A.

Stretching modes

N—H stretching mode was observed at 3351 cm^{-1} (w)[1] (Fig. 3) for both with ATR and KBr techniques (Fig. 4).

C—H stretching vibrations are observed generally in the region 3100–3000 cm^{-1} [18] and they were observed at 3041 cm^{-1} (vw) and 3067[2] cm^{-1} (vw), Ra.

C=O stretching mode was observed at 1653 cm^{-1} (vs) (KBr) (1655 cm^{-1} (vw), Ra). Wavenumber observed at 1516 cm^{-1} (m) (1519 cm^{-1} (vw), Ra) was assigned to N—H bending vibrations.

C=N stretching mode was observed at 1502 cm^{-1} (m) (1500 cm^{-1} (vw), Ra). C—C stretching for ring C was observed only in Raman as very weak intensity peak at 1411 cm^{-1}. C—C stretching for ring A was observed in Raman as very weak intensity peak at 1016 cm^{-1} and 1013 cm^{-1} (vw, Ra). C—N stretching for ring B was observed at 1358 cm^{-1} (vw) (1382 cm^{-1} (vw), Ra). Ring stretching mode for ring C was only observed in Raman spectrum at 1307 cm^{-1} (w). Besides, we have to emphasize that the relative intensities could be different depending on the techniques used (KBr or ATR). Ring stretching modes were observed in MIR spectrum at 1126 cm^{-1} (vw) (1127 cm^{-1} (vw), Ra)), 1118 cm^{-1} (vw), 1096 cm^{-1} (vw) 1106 cm^{-1} (vw), Ra).

C—S stretching mode was observed at 663 cm^{-1} (w) (FIR) and 663 cm^{-1} (w) (MIR). Additional peaks in the 1800–2300 cm^{-1} range and at 1140 cm^{-1} which are due to the diamond crystal used in the ATR unit.

In-plane, out-of-plane bending and torsional modes

C—H in-plane bending vibrations, C—C—H bendings for alkanes and alkenes appear in the 1300–1000 cm^{-1}, 1450–1470 cm^{-1} and 100–650 cm^{-1}, respectively. Out-of-plane bending vibrations occur in the range 1000–750 cm^{-1} for substituted benzenes [25].

The bands observed at 1556 cm^{-1} (vw) (ATR) and 1557 cm^{-1} (vw-Ra) are associated with C—N—H bending mode.

C—C—H in plane bending modes were observed at 1456 (w) (1456 cm^{-1} (s), Ra), 1435 cm^{-1} (m) (KBr) (1436 cm^{-1} (s), Ra), 1408 cm^{-1} (m) (KBr) (1388 cm^{-1} (vw), Ra), 1327 cm^{-1} (w) (1324 cm^{-1} (w) Ra), weak triplet MIR bands at 1284 cm^{-1}/1262 cm^{-1}/1252 cm^{-1} (1285 cm^{-1}/1262 cm^{-1}/1248 cm^{-1}, Ra), another triplets with weak relative intensities at 1181/1171/1161 cm^{-1} (not observed (n.o.) in Ra),

[1] Hereafter, the notations: vs s, m, w, vw, sh, i.p, o.o.p. will stand for: very strong, strong, medium, very weak, shoulder, in-plane and out-of-plane, respectively for the relative intensities for IR and Raman experimental wavenumber values. For clarity, only IR experimental wavenumbers (KBr) and Raman (Ra) spectra are discussed in the text due to the corresponding calculated wavenumbers are already being given in Table 2.

[2] From the calculations, it has seen that these wavenumbers were overestimated due to the selection of proper scaling factor. When double scaling factor is used for this region (above 1800 cm^{-1}), these wavenumbers would be in better agreement with the experimental values [27].

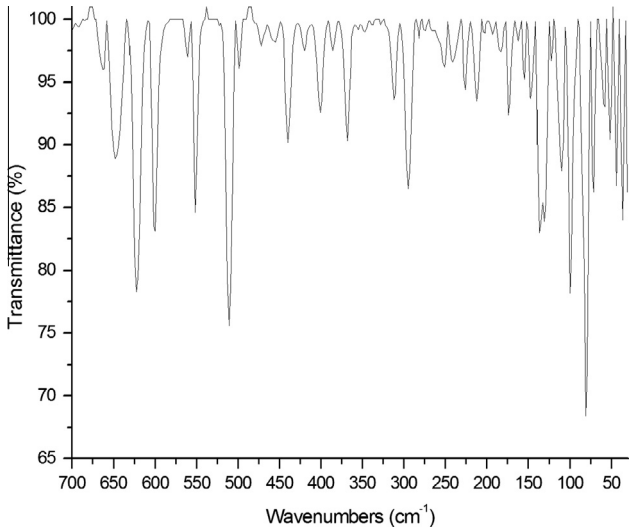

Fig. 2. Far Infrared spectrum of BSN.

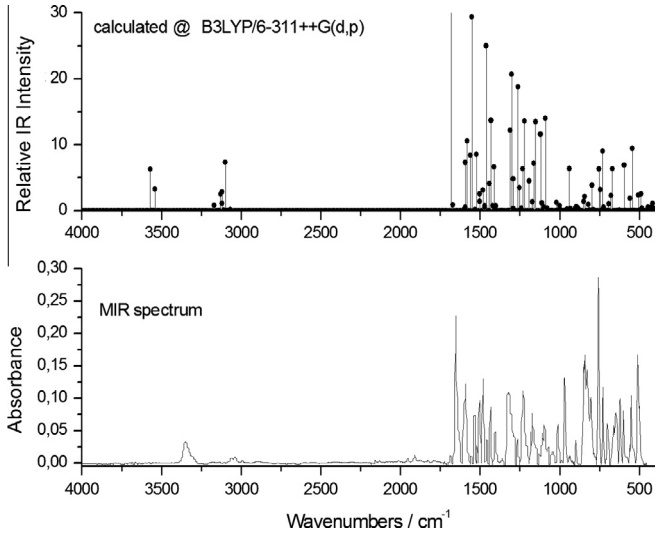

Fig. 3. Calculated vs. experimental spectra of BSN.

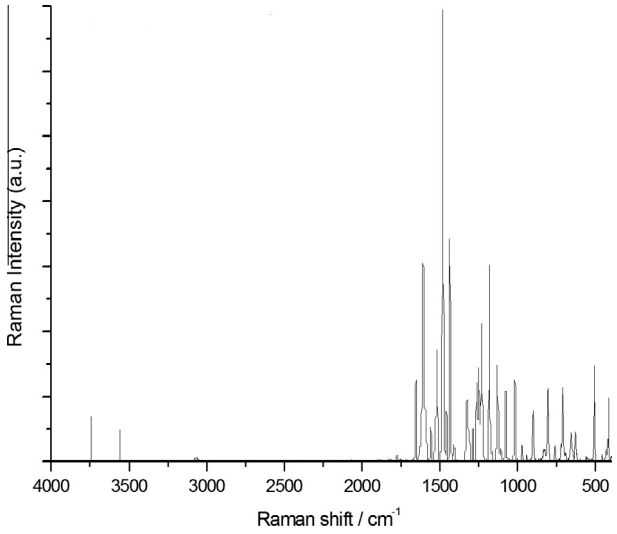

Fig. 4. Experimental Raman spectrum of BSN.

1150 cm^{-1} (vw), 1232 cm^{-1} (m) (1230 cm^{-1} (w), Ra), 1170 cm^{-1} (m) (1161 cm^{-1} (vw), Ra), 1107 cm^{-1} (w) respectively.

C—C—C bendings of the rings D, A and C were observed at 1043 cm^{-1} (vw) (1055 cm^{-1} (vw), Ra), 850 cm^{-1} (vw) (Ra)/ 850 cm^{-1} (m) and 990 cm^{-1} (vw) (993 cm^{-1} (vw), Ra), respectively.

C—N—H bendings were observed at 1556 cm^{-1} (vw)/(1557 cm^{-1} (vw), Ra) and 1483 cm^{-1} (1481 cm^{-1} (vs), Ra).

S—C—N, F—C—C, C—C—N bending modes were observed at 465 cm^{-1} (n.o. in Raman), 392 cm^{-1} (384 cm^{-1} (vw) Ra) and (ring C) 360 cm^{-1} (358 cm^{-1} (vw) Ra), respectively. *Ring stretching mode for ring C* was observed at 1589 cm^{-1} (s) (1590 cm^{-1} (w), Ra). Other wavenumbers that only observed only in Raman and FIR spectra were at 431 cm^{-1} (vw) (440 cm^{-1} (m) FIR), 420 cm^{-1} (vw) (420 cm^{-1} (w)), 415 cm^{-1} (vw) (401 cm^{-1} (m)), 384 cm^{-1} (vw) (385 cm^{-1} (w)), 368 cm^{-1} (vw) (369 cm^{-1} (m)), 358 cm^{-1} (vw) (355 cm^{-1} (vw)), 317 cm^{-1} (vw) (312 cm^{-1} (m)), 298 cm^{-1} (vw) (295 cm^{-1} (m)), 213 cm^{-1} (vw) (212 cm^{-1} (m)), 177 cm^{-1} (vw) 173 cm^{-1} (m)), 155 cm^{-1} (vw) (147 cm^{-1} (m)), 135 cm^{-1} (w) (136 cm^{-1} (m)) and 111 cm^{-1} (w-shoulder) (100 cm^{-1} (s)) correspond to *S—C stretching, C—C—C—C torsion, C—C—C—N torsion, F—C—C i.p. bending, C—C—C—N torsion, C—C—C—C torsion, C—C—C—C torsion, C—C—C o.o.p. bending, C—C—N—C torsion, C—C—N—C torsion, i.p. C—C—C bending and o.o.p. C—C—N—C modes, respectively*.

O—C—N—C o.o.p bending mode was only observed in Raman spectrum at 741 cm^{-1} (vw). Ring torsions (C—C—C—C) were observed at 697 cm^{-1} (vw) in Ra, 701 cm^{-1} (w) KBr/ 701 cm^{-1} (w) ATR), FIR-533 cm^{-1} (vw)/Ra-542 cm^{-1} (vw), KBr-551 cm^{-1} (m)/ ATR 551 cm^{-1} (m)), FIR-511 cm^{-1} (vs)/Ra-507 cm^{-1} (vw)/KBr-502 cm^{-1} (m)/ATR-510 cm^{-1} (s)), FIR-420 cm^{-1} (w)/Ra-420 cm^{-1} (vw)/KBr-418 cm^{-1} (w), FIR-312 cm^{-1} (m)/Ra-317 cm^{-1} and FIR-295 cm^{-1} (m)/Ra-298 cm^{-1}). Ring bending of ring C was observed at 629 cm^{-1}, in Ra. *Only SCN bending* was observed at 472 cm^{-1} (w)-FIR and 465 cm^{-1} (vs)-IR.

C—C—N—H torsions for thiazole ring and C ring respectively were observed at 551 cm^{-1} (s) in FIR, 552 cm^{-1} (vw) in Ra and 540 cm^{-1} (vw) and 267 cm^{-1} (vw) in MIR. Ring A torsion and CCNC torsion, SC stretching, C ring bending, B ring CCCN torsion, FCC bending, modes were observed at 499 cm^{-1} (w)-FIR/497 cm^{-1} (m)-KBr, 456 cm^{-1} (w) in FIR/457 cm^{-1} (vw) in Ra/456 cm^{-1} (m)/458 cm^{-1} (vw) in KBr, 440 cm^{-1} (m)-FIR/431 cm^{-1} (vw) in Ra/426 cm^{-1} (s) in KBr), 401 cm^{-1} (m)-FIR/415 cm^{-1} (vw)-Ra/408 cm^{-1} (w)-KBr and 385 cm^{-1} (w)-FIR/384 cm^{-1} (vw)-Ra, respectively.

Out of plane CH bending modes were observed below 944 cm^{-1}. The modes that only observed in FIR spectrum were at 81 cm^{-1} (vs), 72 cm^{-1} (m), 52 cm^{-1} (m), 44 cm^{-1} (m) and 37 cm^{-1} (m) and correspond to *N—C—C i.p. bending, N—C—C—C torsion (ring D), C—C—C—N* torsion about the bond C_7—C_8, *C—N—C—C, o.o.p. bending* of ring D, respectively.

C—H out of plane (o.o.p) modes were calculated at 819 cm^{-1} (only calc.), observed at 913 cm^{-1} (vw)-ATR), 946 cm^{-1} (only calc.), 729 cm^{-1} (m)-ATR/728 cm^{-1} (s)-KBr/722 cm^{-1} (vw)-Ra, for ring A; 956 cm^{-1} (only calc.), 758 cm^{-1} (s)-KBr/758 cm^{-1} (vs)-ATR/761 cm^{-1} (vw)-Ra, 796 cm^{-1} (only calc.), 899 cm^{-1} (IR)/902 cm^{-1}-Ra for ring C; and 971 cm^{-1} (m)-ATR/970 cm^{-1} (m)-KBr/974 cm^{-1} (vw)-Ra, 937 cm^{-1} (w)-KBr/936 cm^{-1} (vw)-ATR, 805 cm^{-1}(m)-ATR/804 cm^{-1} (w)-KBr/806 cm^{-1} (vw)-Ra, 842 cm^{-1} (s)-ATR/842 cm^{-1} (m)-KBr for ring D, respectively. *N—H o.o.p* mode was only calculated at 266 cm^{-1}. Wavenumbers of BSN-006 observed by FIR spectroscopy below the 700 cm^{-1} range were also given in Table 2. *CCCC torsions* were observed between 542 cm^{-1} and 317 cm^{-1} in Raman spectra. From Table 2, the theoretical predictions fit the experimental observations quite well. The findings given here may be useful for future experimental, such as X-ray, and theoretical studies as alternative progressive investigations.

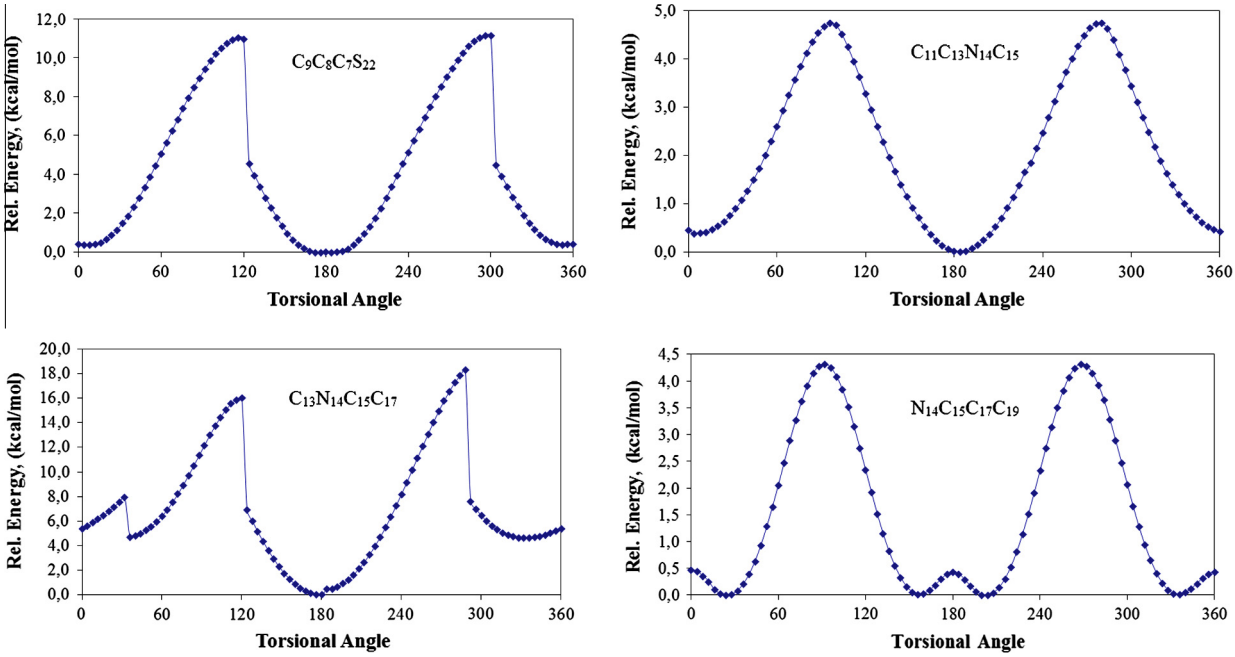

Fig. 5. Energy variation of BSN-006 as a function of defined torsional angles.

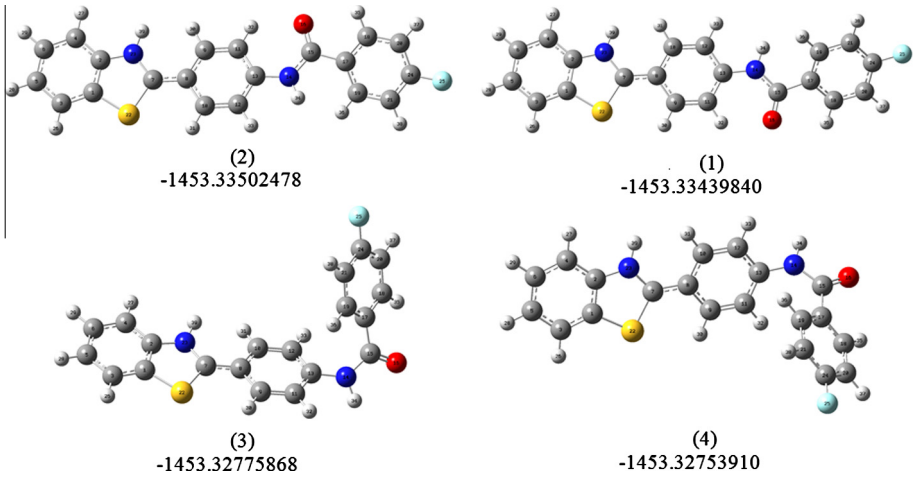

Fig. 6. Most stable conformers of BSN.

Table 3
Energies, relative energies and dipole moments for the conformers.

Parameters	(Conf1)[a]	(Conf2)	(Conf3)	(Conf4)
Energy (kcal/mol)	−1453.3350	−1453.3344	−1453.3277	−1453.3275
Rel. energy (kcal/mol)	0.0000	0.0006	0.0073	0.0075
Dipole moment (Debye)	2.4228	4.9954	5.2697	5.9432
HOMO, LUMO and LUMO–HOMO energy values (in eV) for the conformers				
HOMO energy	−0.13897	−0.13905	−0.14755	−0.14746
LUMO energy	−0.05408	−0.05395	−0.04996	−0.04919
LUMO–HOMO gap	0.08489	0.08510	0.09759	0.09827

[a] Conf: conformer.

Potential energy scan and conformational analysis of BSN-006

Relaxed scans were performed with 4° increments in 90 times. Relaxed scan through the torsional angle coordinates $\tau(C_9C_8C_7S_{22})$, $\tau(C_{11}C_{13}N_{14}C_{15})$, $\tau(C_{13}N_{14}C_{15}C_{17})$ and $\tau(N_{14}C_{15}C_{17}C_{19})$ gives minima corresponding to the conformational isomers (Fig. 5). All the structures obtained near to minima of the scan curves are used as input

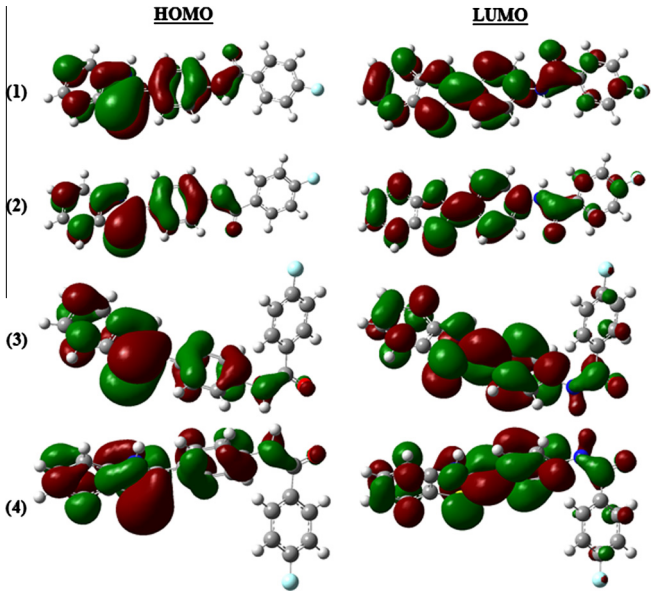

Fig. 7. HOMOs–LUMOs for the most stable conformers of BSN.

to obtain full optimized structures of the conformers. The structures obtained the same conformers from different scans are compared geometrically to eliminate identical structures (Fig. 5). Four stable conformers were obtained for the molecule and shown in Fig. 6. Energies, relative energies and dipole moments with the Highest Occupied Molecular Orbital (HOMO), Lowest Unoccupied Molecular orbital (LUMO) and their differences for the conformers were given in Table 3. HOMO, LUMO structures according to the conformers were given in Fig. 7.

Conclusion

Due to this newly synthesized compound has potent antibacterial and antifungal activities as mentioned in the literature, it is important that analysing the structure and vibrational spectra in detail. In order to do this, vibrational spectroscopic techniques (MIR, FIR, Raman spectroscopic studies) and quantum chemical calculations (DFT/B3LYP/6-311++G(d,p)) were combined, for the first time together for BSN-006. Also, in order to distinguish such compounds derived from such molecules, these combined spectroscopic methods and calculations are inevitably play an important role. Calculations showed that possible Hydrogen bonds formed between carbonyl oxygen atom and environment H atoms of the ring C which shows a potential interactions exist via Hydrogen bonding which leads to derive new compounds such a way. Ring D was seen to be distorted from the plane with a dihedral angle of 26.3°. Potential energy scan and detailed conformational analysis were done on the compound and 4 most stable conformers were determined and their electronic, vibrational and structural properties were presented. All calculated wavenumbers were scaled with 0.978 and results were seen to be in good agreement with experimental IR wavenumbers. Moreover, it might be possible to study any interactions of BSN-006 with other molecular systems as a progressive work via following the procedure given here. In our opinion, the presented experimental observations and the theoretical predictions might be efficient basis for future researches on complexes to be synthesized with the title compound.

Acknowledgements

Acknowledgements to Bolelli K. for supplying the compound, Jose Luis Alonso from University of Valladolid for allowing usage of their high performance clusters for the computation, Sert Y. and Ari H. for recording the micro-Raman and MIR-ATR spectra and other calculations also. Simão A. also acknowledges the Fundação para a Ciência e Tecnologia (FCT, Lisbon, Portugal; Doctoral Grant SFRH/BD/44443/2008, funded by COMPETE-QREN-EU).

References

[1] S.K. Fridkin, R.P. Gaynes, Clin. Chest Med. 20 (2) (1999) 303–316.
[2] G. Trapani, A. Latrofa, M. Franco, D. Armenise, F. Morlacchi, G. Liso, Arzneim. Forsch. 44 (8) (1994) 969–971.
[3] I. Yalcin, I. Oren, E. Aki-Sener, N. Ucarturk, Eur. J. Med. Chem. 27 (1992) 401–406.
[4] I. Yildiz-Oren, I. Yalcin, E. Aki-Sener, N. Ucarturk, Eur. J. Med. Chem. 39 (2004) 291–298.
[5] H. Kucukbay, B. Durmaz, Drug Res. 47 (1997) 667–670.
[6] P.H. Kalina, D.J. Shetlar, R.A. Lewis, L.J. Kullerstrand, R.F. Brubaker, Ophtalmology 95 (1988) 772–777.
[7] R. Paramashivappa, P.P. Kumar, P.V. Subba Rao, A. Rao Srinivasa, Bioorg. Med. Chem. Lett. 13 (2003) 657–660.
[8] J. Koc, V. Klimesova, K. Waisser, J. Kaustova, H.M. Dahse, U. Mollmann, Bioorg. Med. Chem. Lett. 12 (2002) 3275–3278.
[9] L. Katz, Contrib. Schenley Lab. 75 (1953) 712–714.
[10] J. Surin, Southeast Asian J. Trop. Med. Public Health 26 (1) (1995) 128–134.
[11] Y. Komatsu, N. Minami, Chem. Pharm. Bull. 43 (1995) 1614–1616.
[12] T. Kagaya, A. Kajiwara, S. Nagato, K. Akasaka, A. Kubota, J. Pharmacol. Exp. Ther. 278 (1996) 243–251.
[13] I.R. Ager, A.C. Barnes, G.W. Danswan, P.W. Hairsine, D.P. Kay, P.D. Kennewell, S.S. Matharu, P. Miller, P. Robson, D.A. Rowlands, W.R. Tully, R. Westwood, J. Med. Chem. 31 (1988) 1098–1115.
[14] A. Pinar, P. Yurdakul, I. Yildiz-Oren, O. Temiz-Arpaci, N.L. Acan, E. Aki-Sener, I. Yalcin, Biochem. Biophys. Res. Commun. 317 (2) (2004) 670–674.
[15] O. Temiz Arpaci, B. Tekiner-Gulbas, I. Yildiz, E. Aki-Sener, I. Yalcin, Bioorg. Med. Chem. 13 (2005) 6354–6359.
[16] B. Tekiner-Gulbas, O. Temiz Arpaci, I. Yildiz, E. Aki-Sener, I. Yalcin, SAR QSAR Environ. Res. 17 (2) (2006) 121–132.
[17] D.F. Shi, T.D. Bradshaw, S. Wrigley, C.J. McCall, P. Lelieveld, I. Fichtner, M.F.G. Stevens, J. Med. Chem. 39 (1996) 3375–3384.
[18] I. Hutchinson, S.A. Jennings, B.R. Vishnuvajjala, A.D. Westwell, M.F.G. Stevens, J. Med. Chem. 45 (2002) 744–747.
[19] M. Chua, D. Shi, S. Wrigley, T.D. Bradshaw, I. Hutchinson, P.N. Shaw, D.A. Barrett, L.A. Stanley, M.F.G. Stevens, J. Med. Chem. 42 (1999) 381–392.
[20] I. Yalcin, B. Kocyigit-Kaymakcioglu, I. Oren, E. Sener, O. Temiz, A. Akin, N. Altanlar, Il Farmaco 52 (11) (1997) 685–689.
[21] I. Yildiz-Oren, I. Yalcin, E. Aki-Sener, N. Ucarturk, J. Med. Chem. 39 (2004) 291–298.
[22] M.J. Frisch, G.W. Trucks, H.B. Schlegel, G.E. Scuseria, M.A. Robb, J.R. Cheeseman, G. Scalmani, V. Barone, B. Mennucci, G.A. Petersson, H. Nakatsuji, M. Caricato, X. Li, H.P. Hratchian, A.F. Izmaylov, J. Bloino, G. Zheng, J.L. Sonnenberg, M. Hada, M. Ehara, K. Toyota, R. Fukuda, J. Hasegawa, M. Ishida, T. Nakajima, Y. Honda, O. Kitao, H. Nakai, T. Vreven, J.A. Montgomery Jr., J.E. Peralta, F. Ogliaro, M. Bearpark, J.J. Heyd, E. Brothers, K.N. Kudin, V.N. Staroverov, R. Kobayashi, J. Normand, K. Raghavachari, A. Rendell, J.C. Burant, S.S. Iyengar, J. Tomasi, M. Cossi, N. Rega, J.M. Millam, M. Klene, J.E. Knox, J.B. Cross, V. Bakken, C. Adamo, J. Jaramillo, R. Gomperts, R.E. Stratmann, O. Yazyev, A.J. Austin, R. Cammi, C. Pomelli, J.W. Ochterski, R.L. Martin, K. Morokuma, V.G. Zakrzewski, G.A. Voth, P. Salvador, J.J. Dannenberg, S. Dapprich, A.D. Daniels, Ö. Farkas, J.B. Foresman, J.V. Ortiz, J. Cioslowski, D.J. Fox, Gaussian 09, Revision A1, Gaussian, Inc., Wallingford, CT, 2009.
[23] Michal H. Jamroz, Vibrational Energy Distribution Analysis VEDA 4, Warsaw, 2004.
[24] <http://www.chemcraftprog.com>.
[25] K. Bolelli, I. Yalcin, T. Ertan-Bolelli, S. Ozgen, F. Kaynak-Onurdag, I. Yildiz, E. Aki, Med. Chem. Res. 21 (11) (2012) 3818–3825.
[26] B. Stuart, Infrared Spectroscopy: Fundamentals and Applications, Wiley, 2004.
[27] Y. Erdoğdu, O. Unsalan, M. Amalanathan, I. Hubert Joe, J. Mol. Struct. 980 (2010) 24–30.